

**Figure 1.** a) Time-resolved UV/Vis spectra for the reaction between **1** (15 μM) and DHA (15 mM) in the presence of TBAF (22.5 μM) in CH<sub>2</sub>Cl<sub>2</sub> at 25 °C (t = 0 to 70 min). b) Dependence of the log  $k_2'$  values for [1-F]<sup>-</sup> on BDE<sub>(C-H)</sub><sup>[9]</sup> where  $k_2'$  values are normalized per reactive C-H bond.

TBAF, but similarly, negligible spectral changes are found for both [(corrole)Mn<sup>V</sup>(O)]<sup>[16]</sup> and [(porph<sup>+</sup>)Fe<sup>IV</sup>(O)]<sup>[8]</sup> upon addition of axial ligands. Increasing the amounts of TBAF (1000 equiv) result in a further increase in rate, and complete conversion of Mn<sup>V</sup> into Mn<sup>III</sup> occurs in 20 minutes. The decay of Mn<sup>V</sup> (and formation of Mn<sup>III</sup>) followed good pseudo-first-order kinetics for more than three half lives in the presence of excess DHA, thus giving a pseudo-first-order rate constant of  $k_{\text{obs}} = 1.5 \times 10^{-3} \text{ s}^{-1}$ . A plot of  $k_{\text{obs}}$  versus [F<sup>-</sup>] (Figure S1 in the Supporting Information) reveals clear saturation behavior, indicating that a pre-equilibrium step involving F<sup>-</sup> occurs prior to the rate-determining HAT. As shown in Figure S1, excellent linearity is observed for the double-reciprocal plot<sup>[17]</sup> of  $1/[\text{F}^-]_{\text{total}}$  versus  $1/k_{\text{obs}}$ , thus confirming the pre-equilibrium state and yielding  $K = (163 \pm 7) \text{ M}^{-1}$ . The examination of a second C-H substrate (triphenylmethane (TPM), see below) reproduces the same saturation behavior with TBAF (Figure S2 in the Supporting Information) and yields  $K = (191 \pm 10) \text{ M}^{-1}$ , which is in good agreement with the  $K$  value obtained with DHA.<sup>[18]</sup> These results provide good evidence that F<sup>-</sup> coordinates to **1** via the rapid equilibrium **1**

+ F<sup>-</sup> ⇌ [1-F]<sup>-</sup>. This formula is further supported by mass spectrometry data (see below). The most reasonable binding site for F<sup>-</sup> is *trans* to the oxo ligand, as shown in the proposed structure for [1-F]<sup>-</sup> in Scheme 1.

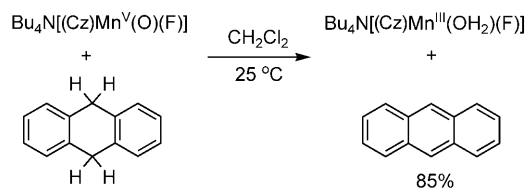
Kinetics for the reaction with DHA under saturating conditions of F<sup>-</sup> (where  $k_{\text{obs}} \approx k_2$  in Scheme 1) were obtained to determine the second-order rate constant ( $k_2'$ ) for [1-F]<sup>-</sup> + DHA. The concentration of DHA was varied, and  $k_{\text{obs}}$  values vary linearly with [DHA] (Figure S3 in the Supporting Information), and is consistent with rate =  $k_2'[[1-F]^-][\text{DHA}]$ . The slope of the best-fit line gives  $k_2'$ , which when corrected for the number of reactive C-H bonds equals  $(3.7 \pm 0.2) \times 10^{-2} \text{ M}^{-1} \text{ s}^{-1}$ . In comparison, **1** + DHA in the absence of fluoride reacts with a rate constant of  $k_2' = (1.8 \pm 0.5) \times 10^{-5} \text{ M}^{-1} \text{ s}^{-1}$ . Thus, the addition of a fluoride anion induces a remarkable rate-enhancement of  $k_2'([\text{1-F}]^-)/k_2'(\mathbf{1}) = 2100$  for hydrogen-atom abstraction (Table 1). Product analysis by gas chromatography (GC) of the oxidation of DHA showed that anthracene was the major product (85% yield; Scheme 2), thus confirming HAT by [1-F]<sup>-</sup>, and supporting the stoichiometry predicted in Scheme 1. A significant kinetic isotope effect of  $k_2'_{\text{H}}/k_2'_{\text{D}} = 10.5$  for DHA versus [D<sub>4</sub>]DHA was also obtained, further supporting HAT as the rate-determining step.

A range of C-H substrates with different bond strengths (bond dissociation energies = BDEs) were next examined to gain further insights into the mechanism of oxidation. The oxidation of these substrates with **1** + TBAF (1000 equiv) in CH<sub>2</sub>Cl<sub>2</sub> under anaerobic conditions at 25 °C led to the isosbestic transformation of [1-F]<sup>-</sup> into [2-F]<sup>-</sup>, and showed a

**Table 1:** Comparison of second-order rate constants for **1**, [1-F]<sup>-</sup>, and [1-CN]<sup>-</sup>.

Substrate	$k_2' [\text{M}^{-1} \text{ s}^{-1}]^{\text{[a]}}$				
	<b>1</b>	[1-F] <sup>-</sup>	$\frac{k_2'([\text{1-F}]^-)}{k_2'(\mathbf{1})}$	[1-CN] <sup>-</sup>	$\frac{k_2'([\text{1-CN}]^-)}{k_2'(\mathbf{1})}$
indene		0.27 ± 0.02		27 ± 1	
xanthene		0.18 ± 0.04		3.6 ± 0.5	
9,10-dihydroanthracene	$(1.8 \pm 0.5) \times 10^{-5}$	$(3.7 \pm 0.2) \times 10^{-2}$	2100	0.29 ± 0.02	16 000
1,4-cyclohexadiene	$(3.3 \pm 0.1) \times 10^{-5}$	$(2.5 \pm 0.1) \times 10^{-2}$	760	0.27 ± 0.01	8200
triphenylmethane		$(6.6 \pm 0.2) \times 10^{-4}$			

[a] Rate constants are normalized per reactive C-H bond. [b] Experimental and calculated (in square brackets) kinetic isotope effect (KIE) values for the reaction with DHA versus [D<sub>4</sub>]DHA.



**Scheme 2.** Reaction of [1-F]<sup>-</sup> with DHA.

second-order dependence on the substrate.<sup>[20]</sup> A plot of BDE<sub>(C-H)</sub> versus log  $k_2'$  reveals a linear correlation (Figure 1b), often characteristic of HAT reactions.<sup>[21]</sup> The slope ( $-0.42 \pm 0.05$ ) is in good agreement with other metal-oxo



intermediate **Int**, which then abstracts a second hydrogen-atom via the transition state **TS<sub>D</sub>** to form anthracene and Mn<sup>III</sup> as products (**Prod**). Calculated free energy values show that the first hydrogen-atom abstraction barrier (**TS<sub>HA</sub>**) is rate-determining, and is in agreement with the experimental finding that there is no observable build-up of a Mn<sup>IV</sup> intermediate. A triplet spin state <sup>3</sup>[(Cz)Mn(O)] (spin densities reveal a [(Cz<sup>+</sup>)Mn<sup>IV</sup>(O)] configuration) lies well above the ground state for the reactants by 6.2–9.5 kcal mol<sup>-1</sup>, but does react to form a radical intermediate <sup>3</sup>**Int** with the same orbital occupation as the singlet; [(Cz)Mn<sup>IV</sup>(OH)]–[DHA-H]. The potential energy profiles for the triplet states for **1**, [1-F]<sup>-</sup>, and [1-CN]<sup>-</sup> (Figures S15–S17 in the Supporting Information) reveal transition states <sup>3</sup>**TS<sub>HA</sub>** slightly higher in energy (0.8–1.6 kcal mol<sup>-1</sup>) than the corresponding singlet states <sup>1</sup>**TS<sub>HA</sub>**. The singlet and triplet states become nearly degenerate upon reaching the intermediate, **Int**, and therefore a spin-state crossing may occur, but only following the initial hydrogen-atom abstraction barrier **TS<sub>HA</sub>**. Hence, the reactivity of **1**, [1-F]<sup>-</sup>, and [1-CN]<sup>-</sup> toward HAT are not influenced by a spin-state crossing mechanism. Optimized geometries of **TS<sub>HA</sub>** are shown in Figure 2. Without an axial ligand, the barrier is late with short O–H and long C–H bond lengths, which is typical for high-barrier transition states.<sup>[23]</sup>

The lack of multistate reactivity for **1** is in contrast to HAT reactions involving many other heme and nonheme metal-oxo species, for which multistate reactivity has been invoked as a critical factor.<sup>[7,24]</sup> These results also contrast recent theoretical work on Mn<sup>V</sup>(O) porphyrins, for which multistate reactivity has been suggested.<sup>[25]</sup> Interestingly, the singlet state of Mn<sup>V</sup>(O) porphyrins was found completely unreactive toward HAT, but our calculations suggest that the Mn<sup>V</sup>(O) corrolazines, in contrast, likely operate via a novel single-state-reactivity pathway.

What is most striking from DFT calculations is the dramatic lowering of the initial HAT barrier (**TS<sub>HA</sub>**) upon the coordination of F<sup>-</sup> or CN<sup>-</sup> to **1** (7.4 and 9.7 kcal mol<sup>-1</sup> lower than **1**, respectively). The trend in reactivity, [1-CN]<sup>-</sup> > [1-F]<sup>-</sup> ≫ **1**, predicted in Figure 2 by the relative HAT barriers (**TS<sub>HA</sub>**) is in excellent agreement with the experimental rate constants for DHA oxidation. Calculated KIE values of 8.5 and 8.6 for hydrogen-abstraction by [1-F]<sup>-</sup> and [1-CN]<sup>-</sup>, respectively, correspond well with the experimental findings (Table 1).

What drives the lowering of the HAT barrier upon addition of anionic donors? A clue comes from the stability of the <sup>1</sup>**Int** intermediate, which increases significantly upon coordination of F<sup>-</sup> or CN<sup>-</sup>. The C–H activation step for nonligated **1** is endothermic, whereas the same step for [1-F]<sup>-</sup> and [1-CN]<sup>-</sup> is strongly exothermic. Because reaction exothermicity and barrier height often correlate with each other,<sup>[26]</sup> it is important to determine the possible factors that influence the stability of <sup>1</sup>**Int**. Calculation of the O–H bond strength for <sup>1</sup>[(Cz)Mn<sup>IV</sup>(OH)] gives a BDE<sub>OH</sub> = 69.3 kcal mol<sup>-1</sup>, which dramatically increases to 81.7 and 86.7 kcal mol<sup>-1</sup> for the systems with F<sup>-</sup> or CN<sup>-</sup>, respectively. These values predict that the exothermicity of HAT should increase by 12.4 and 17.4 kcal mol<sup>-1</sup>, respectively, as a result of addition of F<sup>-</sup> or CN<sup>-</sup>. Recent studies of hydrogen-abstrac-

tion reactions by a range of iron(IV)–oxo oxidants implicated a linear correlation of barrier height with BDE<sub>OH</sub>,<sup>[27]</sup> in agreement with the trend observed here (Figure S20 in the Supporting Information). Mayer et al. have shown that the BDEs and rates of HAT for metal complexes correlate with simple organic radicals.<sup>[21]</sup> A plot of the theoretical BDE<sub>OH</sub> values versus experimental log *k* for the reactions of **1**, [1-F]<sup>-</sup>, and [1-CN]<sup>-</sup> with DHA fits remarkably well with the data for the organic radicals *sec*-BuO<sub>2</sub><sup>•</sup> and *t*BuO<sup>•</sup>, thereby enhancing the validity of the BDEs derived from DFT (Figure 3).

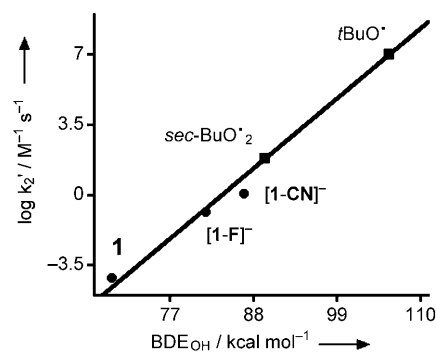


**Figure 3.** Plot of DFT calculated BDE<sub>OH</sub> values versus experimental log *k*<sub>2</sub>' values for the reaction of **1**, [1-F]<sup>-</sup>, and [1-CN]<sup>-</sup> with DHA. Best-fit line through data for *sec*-BuO<sub>2</sub><sup>•</sup> and *t*BuO<sup>•</sup>.<sup>[21]</sup>

A thermodynamic analysis<sup>[21]</sup> shows that the strength of the O–H bond in <sup>1</sup>[(Cz)Mn<sup>IV</sup>(OH)] is proportional to the electron affinity (EA) of the Mn<sup>V</sup>(O) complex and the proton affinity of the hypothetical one-electron-reduced [Mn<sup>IV</sup>(O)]<sup>-</sup> species. The EA values for **1**, [1-F]<sup>-</sup>, and [1-CN]<sup>-</sup> obtained by DFT calculation (Table S14 in the Supporting Information) reveal a significant decrease (11.3–14.0 kcal mol<sup>-1</sup>) upon addition of the anionic axial donors compared to **1**, which should induce a weakening of the O–H bond in the Mn complex. Thus, according to the DFT calculations, the large increase in BDE<sub>OH</sub> must arise from a substantial increase in proton affinity (26.4–28.7 kcal mol<sup>-1</sup>) upon addition of F<sup>-</sup> or CN<sup>-</sup>. In other words, the basicity of [Mn<sup>IV</sup>(O)]<sup>-</sup>, not the oxidizing power of the Mn<sup>V</sup>(O) complex, is predicted to be greatly enhanced by axial ligation and leads to the dramatic increase in reactivity.<sup>[28]</sup>

These results are in concert with the notion that the Cys ligand in Cyt-P450 may serve to enhance the basicity of the iron–oxo intermediate, thereby providing a means for the activation of inert C–H bonds in the presence of an oxidatively susceptible protein matrix. Interestingly, recent DFT calculations on Cyt-P450 suggest that the anionic Cys donor induces similar opposing effects on electron affinity and proton affinity.<sup>[29]</sup> Further studies to understand the influence of ancillary ligands on metal–oxo HAT reactions in both synthetic and biological systems are clearly warranted.

Received: February 26, 2010

Revised: April 21, 2010

Published online: June 16, 2010

**Keywords:** hydrogen-atom transfer · ligand effects · manganese · metalloenzymes · porphyrinoids

- [1] a) M. T. Green, *Curr. Opin. Chem. Biol.* **2009**, *13*, 84–88; b) M. T. Green, J. H. Dawson, H. B. Gray, *Science* **2004**, *304*, 1653–1656.
- [2] a) M. H. V. Huynh, T. J. Meyer, *Chem. Rev.* **2007**, *107*, 5004–5064; b) J. M. Mayer, *Annu. Rev. Phys. Chem.* **2004**, *55*, 363–390; c) S. Y. Reece, D. G. Nocera, *Annu. Rev. Biochem.* **2009**, *78*, 673–699; d) M. T. Caudle, V. L. Pecoraro, *J. Am. Chem. Soc.* **1997**, *119*, 3415–3416.
- [3] C. Arunkumar, Y. M. Lee, J. Y. Lee, S. Fukuzumi, W. Nam, *Chem. Eur. J.* **2009**, *15*, 11482–11489.
- [4] S. R. Bell, J. T. Groves, *J. Am. Chem. Soc.* **2009**, *131*, 9640–9641.
- [5] Y. Kang, H. Chen, Y. J. Jeong, W. Lai, E. H. Bae, S. Shaik, W. Nam, *Chem. Eur. J.* **2009**, *15*, 10039–10046.
- [6] T. H. Parsell, M. Y. Yang, A. S. Borovik, *J. Am. Chem. Soc.* **2009**, *131*, 2762–2763.
- [7] C. V. Sastri, J. Lee, K. Oh, Y. J. Lee, J. Lee, T. A. Jackson, K. Ray, H. Hirao, W. Shin, J. A. Halfen, J. Kim, L. Que, Jr., S. Shaik, W. Nam, *Proc. Natl. Acad. Sci. USA* **2007**, *104*, 19181–19186.
- [8] A. Takahashi, T. Kurahashi, H. Fujii, *Inorg. Chem.* **2009**, *48*, 2614–2625.
- [9] G. C. Yin, A. M. Danby, D. Kitko, J. D. Carter, W. M. Scheper, D. H. Busch, *J. Am. Chem. Soc.* **2007**, *129*, 1512–1513.
- [10] R. Zhang, J. H. Horner, M. Newcomb, *J. Am. Chem. Soc.* **2005**, *127*, 6573–6582.
- [11] D. P. Goldberg, *Acc. Chem. Res.* **2007**, *40*, 626–634.
- [12] I. Aviv, Z. Gross, *Chem. Commun.* **2007**, 1987–1999.
- [13] D. E. Lansky, B. Mandimutsira, B. Ramdhanie, M. Clausén, J. Penner-Hahn, S. A. Zvyagin, J. Telsler, J. Krzystek, R. Q. Zhan, Z. P. Ou, K. M. Kadish, L. Zakharov, A. L. Rheingold, D. P. Goldberg, *Inorg. Chem.* **2005**, *44*, 4485–4498.
- [14] D. E. Lansky, D. P. Goldberg, *Inorg. Chem.* **2006**, *45*, 5119–5125.
- [15] This spectrum (Figure S5 in the Supporting Information) is similar to the UV/Vis spectrum of the chloride-ligated complex Et<sub>4</sub>N[(TBP<sub>8</sub>Cz)Mn<sup>III</sup>(Cl)], which has been definitively characterized by X-ray crystallography, see: D. E. Lansky, A. A. N. Sarjeant, D. P. Goldberg, *Angew. Chem.* **2006**, *118*, 8394–8397; *Angew. Chem. Int. Ed.* **2006**, *45*, 8214–8217).
- [16] H. Y. Liu, H. Zhou, L. Y. Liu, X. Ying, H. F. Jiang, C. K. Chang, *Chem. Lett.* **2007**, *36*, 274–275.
- [17] M. R. Wright, *An Introduction to Chemical Kinetics*, Wiley, Chichester, **2004**.
- [18] The accuracy of these binding constants, however, should be interpreted with caution because they are derived indirectly from kinetic data.
- [19] For sources of BDE<sub>(C–H)</sub> values, see Figure S4 in the Supporting Information.
- [20] GC analysis showed the expected products for oxidation of 1,4-cyclohexadiene (benzene), xanthene (xanthone), and triphenylmethane (triphenylmethanol).
- [21] J. M. Mayer, E. A. Mader, J. P. Roth, J. R. Bryant, T. Matsuo, A. Dehestani, B. C. Bales, E. J. Watson, T. Osako, K. Valliant-Saunders, W. H. Lam, D. A. Hrovat, W. T. Borden, E. R. Davidson, *J. Mol. Catal. A* **2006**, *251*, 24–33.
- [22] S. Cai, S. Licoccia, F. A. Walker, *Inorg. Chem.* **2001**, *40*, 5795–5798.
- [23] S. Shaik, D. Kumar, S. P. de Visser, *J. Am. Chem. Soc.* **2008**, *130*, 10128–10140.
- [24] a) S. P. de Visser, L. Tahsini, W. Nam, *Chem. Eur. J.* **2009**, *15*, 5577–5587; b) D. Kumar, H. Hirao, L. Que, Jr., S. Shaik, *J. Am. Chem. Soc.* **2005**, *127*, 8026–8027; c) S. Shaik, D. Kumar, S. P. de Visser, A. Altun, W. Thiel, *Chem. Rev.* **2005**, *105*, 2279–2328.
- [25] D. Balcells, C. Raynaud, R. H. Crabtree, O. Eisenstein, *Inorg. Chem.* **2008**, *47*, 10090–10099.
- [26] M. G. Evans, M. Polanyi, *Trans. Faraday Soc.* **1936**, *32*, 1333–1359.
- [27] S. P. de Visser, *J. Am. Chem. Soc.* **2010**, *132*, 1087–1097.
- [28] For a recent example of an iron–imido complex where the high basicity provides the driving force for HAT, see: I. Nieto, F. Ding, R. P. Bontchev, H. B. Wang, J. M. Smith, *J. Am. Chem. Soc.* **2008**, *130*, 2716–2717.
- [29] A. Dey, Y. I. Jiang, P. O. de Montellano, K. O. Hodgson, B. Hedman, E. I. Solomon, *J. Am. Chem. Soc.* **2009**, *131*, 7869–7878.